Mode-3 spontaneous crack propagation along functionally graded bimaterial interfaces

Kubair, D. V. * Bhanu-Chandar, B.,

Computational Dynamic Fracture Mechanics Laboratory, Department of Aerospace Engineering, Indian Institute of Science, Bangalore-560012

Abstract

The effects of combining functionally graded materials of different inhomogeneous property gradients on the mode-3 propagation characteristics of an interfacial crack are numerically investigated. Spontaneous interfacial crack propagation simulations were performed using the newly developed spectral scheme. The numerical scheme derived and implemented in the present work can efficiently simulate planar crack propagation along functionally graded bimaterial interfaces. The material property inhomogeneity was assumed to be in the direction normal to the interface. Various bimaterial combinations were simulated by varying the material property inhomogeneity length scale. Our parametric study showed that the inclusion of a softening type functionally graded material in the bimaterial system leads to a reduction in the fracture resistance indicated by the increase in crack propagation velocity and power absorbed. An opposite trend of increased fracture resistance was predicted when a hardening material was included in the bimaterial system. The cohesive tractions and crack opening displacements were altered due to the material property inhomogeneity, but the stresses ahead of the cohesive zone remained unaffected.

Key words: functionally graded materials, multi-functional materials, bimaterial systems, interfacial crack propagation, inhomogeneity length scale, anti-plane shear, spectral scheme, cohesive zone model, spontaneous crack propagation.

1 Introduction

Functionally graded materials (FGMs) are composites that have smoothly varying material properties as a function of the spatial position. Examples

* coressponding author. Tel.:+91-080-2293-3035; Fax:+91-080-2360-0134.
Email address: kubair@aero.iisc.ernet.in (Kubair, D. V.).

Article accepted in Journal of the Mechanics and Physics of Solids (2006) 1–25

of naturally occurring functionally graded materials include bones and wood (Suresh and Mortensen, 1998). Achieving inhomogeneous material properties by case hardening to increase wear resistance is a common engineering example of a functionally graded material. The concept of functionally graded materials originated from the need of a material that could be used as a thermal barrier coating in gas turbines and rocket nozzles (Koizumi and Niino, 1995; Koizumi, 1997; Movchan and Yakovchuk, 2004). Functionally graded materials used in thermal barrier coatings were manufactured by combining ceramics and metals so as to achieve high-toughness at high-temperatures. Current applications of functionally graded materials include wear resistance coatings (Schulz et al., 2003; Gasik et al., 2003; Put et al., 2003; Melgarejo et al., 2006), manufacture of microelectromechanical systems MEMS (Witvrouw and Mehta, 2005), sensors (Muller et al., 2003) and biological implants (Pompe et al., 2003; Watari et al., 2004; Zhang et al., 2005). Graded materials have also found applications in electronic components (Wosko et al., 2005; Kato et al., 2006). Similar to the multitude of applications, there are a variety of manufacturing techniques that can produce functionally graded materials. These include controlled exposure to ultraviolet radiation (Lambros et al., 1999), using laser melt injection (Hosson and Ocelik, 2003), centrifugal molding (Chen et al., 2005; Watanabe et al., 2005), dynamic shock compression (van Zyl et al., 2005), spark plasma sintering (Kondo et al., 2004; Jiang et al., 2005), pressureless sintering (Pine and Bruck, 2006) and by controlled suspension of particles in polymer matrices (Hashmi, 2006; Kirugulige and Tippur, 2006; Kitey and Tippur, 2005). From the above mentioned examples it is clear that the concepts of manufacturing and applications of functionally graded materials are well established. However, testing methods and design methodologies using these novel materials is not well developed and needs a thorough understanding of the failure mechanics of FGMs. Particular to the present study the effect of material inertia and mismatch in the material property gradient is not well understood on the fracture behaviour of functionally graded materials and forms as the primary motivation.

The earliest work on fracture mechanics analysis of functionally graded materials was by Delale and Erdogan (1983). They analysed a stationary crack embedded in an elastic functionally graded material. Their analysis concluded that stress-intensity-factor (SIF) based design methodology, which is popular in homogeneous materials to be sufficient even in case of FGMs. Their idea was supported by Eischen (1987), whose asymptotic analysis around a stationary crack in a FGM showed that the stress-singularity remains unaffected by the varying material property gradation. Asymptotic analysis of Parameswaran and Shukla (2002) has shown that the material property variation affects only the higher order terms for a stationary crack. There are a few experimental studies available in the literature that have addressed crack along functionally graded bimaterials. Marur and Tippur (2000) have performed impact experiments on epoxy based graded materials to extract the time history of

the mixed-mode stress intensity factors. Their experiments showed that the mode-mixity was altered due to the material property gradient. Kirugulige and Tippur (2006) have experimentally found that the inhomogeneous material property variation alters the kinking of a mixed-mode crack in their glass-filled epoxy specimen. They observed that kinking is significant when a crack grows into a progressively stiffer (increase in Young's modulus) FGM. Jain and Shukla (2006) have performed dynamic fracture experiments on different FGM specimen geometries. Their study on particulate filled functionally graded materials showed that the crack propagation velocities increased, while the crack arrest toughness was reduced compared to a homogeneous material. Abanto-Bueno and Lambros (2006) have performed crack propagation experiments on specimen manufactured by ultraviolet irradiation. Their experiments showed that the kinking criterion for inhomogeneous materials to be different from that of the maximum hoop stress criterion used in homogeneous materials. Owing to the complexity of the analysis only a few studies are available that address the issue of dynamic fracture along functionally graded bimaterial interfaces. Ma et al. (2005) have used a Fourier transform method to extract the mixed-mode stress intensity factors in their analysis. Feng et al. (2005) have analysed torsional impact on a functionally graded interlayer system and concluded that the dynamic stress intensity factor is altered by the material property inhomogeneity. Lee and Choi (2006) have analysed the mode-3 impact problem solving a Cauchy singular integral equation. They extracted the stress intensity factors for a stationary crack along the interface of a functionally graded bimaterial system. Most of the above mentioned analyses have considered stationary cracks subjected to transient loading and described the effect of the material property inhomogeneity on the dynamic stress intensity factor. In a recent study, our group had performed spectral simulations of spontaneous crack propagation in functionally graded materials. In those analyses we had assumed the material property variation to be either unsymmetric (Kulkarni et al., 2007) or symmetric (Pal et al., 2007) about the crack propagation plane. Our analyses had shown that the inhomogeneous material property variation affected the crack propagation characteristics such as velocity, acceleration and the energetics. For the sake of simplicity we had assumed that the inhomogeneity to be identical on either side of the crack propagation plane. In the present work we extend our analysis to address the issue of spontaneous crack propagation along functionally graded bimaterial interfaces.

There are several numerical tools that researchers have implemented and used to simulate crack propagation in homogeneous and functionally graded materials. These include finite differences (Yang and RaviChandar, 1996; Mikumo et al., 1987) , cohesive volume finite elements (Xu and Needleman, 1994; Camacho and Ortiz, 1996; Geubelle and Baylor, 1998; Kandula et al., 2005) , finite elements (Tilbrook et al., 2005) and boundary integral methods. As mentioned earlier, we focus our attention on describing the effect of material

property inhomogeneity on the crack propagation characteristics. Hence, we restrict our attention to planar crack propagation (no kinking) under anti-plane shear loading. In the present study we develop a new spectral scheme based on the bimaterial formulation of Geubelle and Breitenfeld (1997). The spectral scheme developed here can simulate spontaneous crack propagation along functionally graded bimaterial interfaces. The novelty of the spectral scheme is its versatility in handling different types of state- and rate-dependent cohesive laws (Kubair et al., 2003; Kubair and Geubelle, 2003). The details of the derivation of the spectral form of the elastodynamic equations are presented in Section 2. In Section 3, we present the details of the numerical implementation of the spectral scheme. The developed numerical tool is used to perform spontaneous crack propagation simulations along the interface of several functionally graded bimaterial combinations and the results from our simulations are discussed in Section 4.

2 Formulation

In this section the elastodynamic relation for an inhomogeneous bimaterial system are derived. The model elastodynamic problem considered in this study is depicted in Figure 1. An interfacial crack of initial length a_o is allowed to

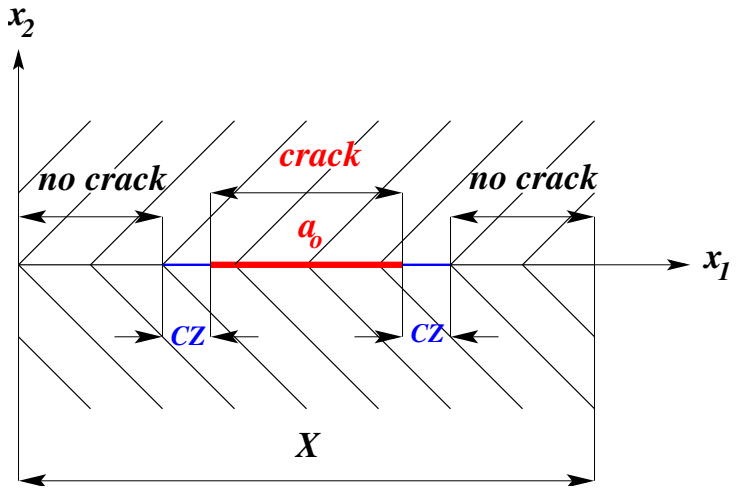

Fig. 1. Geometry of the functionally graded bimaterial system. The three distinct regions on the weak-plane ($x_2 = 0$) are shown corresponding to the crack, cohesive zone (CZ) and the uncracked portion.

propagate spontaneously on the weak-plane due to the action of an arbitrary spatial- and time-dependent mode-3 loading of amplitude τ_o. Similar to the experiments of Xu et al. (2003) and Lambros and Rosakis (1995) the bimaterial interface (weak plane) is assumed to be prepared by gluing two half-spaces (inhomogeneous) with an appropriate adhesive leading to a sharp interface.

The materials above and below the weak-plane are designated by a plus (+) and minus (-), respectively. Motivated by the experiments of Kirugulige and Tippur (2006) and Jain and Shukla (2006), the rigidity modulus (μ) and density (ρ) in the two half-spaces are allowed to vary exponentially in the direction perpendicular to the weak-plane as

$$\begin{aligned} \mu\left(x_2^{\pm}\right) &= \mu_o^{\pm} \exp\left(\frac{x_2^{\pm}}{L_g^{\pm}}\right), \\ \rho\left(x_2^{\pm}\right) &= \rho_o^{\pm} \exp\left(\frac{x_2^{\pm}}{L_g^{\pm}}\right), \end{aligned} \tag{1}$$

where $\mu_o^{\pm}$ and $\rho_o^{\pm}$ are the rigidity modulus and density on the weak-plane ($x_2 = 0$) for the top (+) and bottom (-) materials, respectively. In the present bimaterial formulation, the material properties are allowed to suffer a discontinuous jump across the weak-plane. In Equation (1) $L_g^{\pm}$ corresponds to the natural inhomogeneity length scale of the FGM, which controls how fast or slow the material properties vary along the $x_2^{\pm}$ direction. The inhomogeneity length scale L_g can be in the order of a few microns (as the case of thermal barrier coatings and layered solids) or in the order of several meters as in tectonic plates. Unlike in the previous FGM formulations by Kulkarni et al. (2007) and Pal et al. (2007), the inhomogeneity length scales are allowed to vary independently in either of the two half-spaces. The trivial case of a homogeneous material is obtained by assuming $L_g^{\pm} = \pm\infty$. The inhomogeneity length scale can be either positive or negative in our formulation. In the upper half-space a positive value of the inhomogeneity length scale leads to an inhomogeneous material that progressively becomes more rigid (μ increases) and denser away from the weak-plane and is termed as a "hardening" or "strengthening" type functionally graded material. When the inhomogeneity length scale is set to be less than zero (that is negative) the material properties degenerate away from the weak-plane and hence called a "softening" or "weakening" type functionally graded material. A combination of a softening material in one half and a hardening material in the other with different inhomogeneities (different $L_g^{'s}$) is possible in the present bimaterial formulation. The particular case of the unsymmetric (Kulkarni et al., 2007) functionally graded material can be obtained by assuming $\mu_o^+ = \mu_o^-$, $\rho_o^+ = \rho_o^-$ with $L_g^+ = L_g^-$. Similarly, a symmetric functionally graded material (Pal et al., 2007) can be obtained by assuming $\pm L_g^+ = \mp L_g^-$, with identical rigidity moduli and densities for the two half-spaces. As mentioned earlier, in the present bimaterial formulation we allow the material properties, namely the rigidity moduli (μ), densities (ρ) and the inhomogeneity length scale (L_g) to be independently different in the two half-spaces. As seen from Equation (1), the inhomogeneous variation of the rigidity modulus and densities in the two half-spaces are assumed to be identical mathematical functions similar to the analysis and experiments of Jain and Shukla (2006) and Kirugulige and Tippur (2006). This assumption leads to a homo-

geneous shear wave speed $c_s^{\pm} = \sqrt{\mu_o^{\pm}/\rho_o^{\pm}}$ in each of the half-spaces. We start our derivation of the spectral formulation from the conservation of linear momentum written in terms of the only non-vanishing out-of-plane displacements $u_3^{\pm}$, which is given by

$$\frac{\partial^2 u_3^{\pm}}{\partial x_1^2} + \frac{\partial^2 u_3^{\pm}}{\partial x_2^2} + \frac{1}{L_g^{\pm}} \frac{\partial u_3^{\pm}}{\partial x_2} = \frac{1}{\left(c_s^{\pm}\right)^2} \frac{\partial^2 u_3^{\pm}}{\partial t^2}, \tag{2}$$

where t is the time coordinate. Equation (2) is a second order hyperbolic equation and will assume the canonical form of a scalar wave equation when the inhomogeneity length scale $L_g^{\pm} = \pm\infty$ (a homogeneous material). The out-of-plane displacement is transformed into the Fourier and Laplace domains as

$$\hat{\psi}^{\pm}\left(k, x_2^{\pm}, p\right) = \int_{t=0}^{t=\infty} \int_{x_1=-\infty}^{x_1=\infty} u_3^{\pm}\left(x_1, x_2^{\pm}, t\right) \exp\left(-ikx_1 - pt\right) dx_1 dt, \tag{3}$$

where k's are the spectral mode numbers (assumed to real constants) and p is the complex Laplace transform variable. The conservation of linear momentum (2) can be written as an ordinary differential equation in the transformed space as

$$\frac{d^2 \hat{\psi}^{\pm}}{dx_2^2} + \frac{1}{L_g^{\pm}} \frac{d\hat{\psi}^{\pm}}{dx_2} - k^2 \left(1 + \left(\frac{p}{k c_s^{\pm}}\right)^2\right) \hat{\psi}^{\pm} = 0. \tag{4}$$

The solution to the above equation can be written as

$$\hat{\psi}^{\pm} = C_1^{\pm} \exp\left(m_1^{\pm} x_2\right) + C_2^{\pm} \exp\left(m_2^{\pm} x_2\right), \tag{5}$$

where $C_1^{\pm}$ and $C_2^{\pm}$ are arbitrary constants determined by appropriate boundary conditions, while $m_1^{\pm}$ and $m_2^{\pm}$ are the roots of the underlying characteristic equation (4) and are given by

$$m_{1/2}^{\pm} = \frac{1 \pm \sqrt{1 + 4k^2 \left(L_g^{\pm}\right)^2 \left(1 + \frac{p^2}{k^2 \left(c_s^{\pm}\right)^2}\right)}}{2 L_g^{\pm}} \tag{6}$$

In order to obtain a bounded solution for the stresses and displacements in both the half-spaces, we choose the branch of the solution that is less than zero as

$$m^{\pm} = \min\left(\left[\operatorname{sign}\left(L_g^{\pm}\right) \operatorname{sign}\left(x_2\right) m_1^{\pm}\right], \left[\operatorname{sign}\left(L_g^{\pm}\right) \operatorname{sign}\left(x_2\right) m_2^{\pm}\right]\right) \tag{7}$$

The bounded solution in the two half-spaces can now be written as

$$\hat{\psi}^{\pm} = \hat{\psi}_o^{\pm} \exp\left(m^{\pm} x_2\right), \tag{8}$$

where $\hat{\psi}_o^{\pm} = \hat{\psi}^{\pm}\left(k, x_2 = 0^{\pm}, p\right)$. In order to obtain the boundary integral equation on the weak-plane we define the traction $\tau\left(x_1, t\right) = \sigma_{23}\left(x_1, x_2 = 0, t\right)$ in the transformed plane as

$$\hat{T}\left(k, p\right) = \int_{t=0}^{t=\infty} \int_{x_1=-\infty}^{x_1=\infty} \tau\left(x_1, t\right) \exp\left(-ikx_1 - pt\right) dx_1 dt. \tag{9}$$

The tractions and the displacements on the weak-plane are related through the constitutive relation as

$$\hat{T} = \mp \mu_o^{\pm} m^{\pm} \hat{\psi}_o^{\pm}. \tag{10}$$

The two half-spaces tend to separate at the instant a remote external load is applied on the weak-plane, which are restrained by the action of the cohesive tractions. The elastodynamic relation (10) is modified by superposing the tractions due to the instantaneous slipping as

$$\hat{T} = \mp \frac{\mu_o^{\pm}}{c_s^{\pm}} p \hat{\psi}_o^{\pm} \mp \mu_o^{\pm} \left|k\right| \left(\frac{m^{\pm}}{\left|k\right|} - \frac{p}{\left|k\right| c_s^{\pm}}\right) \hat{\psi}_o^{\pm}. \tag{11}$$

Inverting the above and superposing an external traction $\tau_o\left(x_1, t\right)$, the traction in the x_1-t space is written as

$$\tau\left(x_1, t\right) = \tau_o\left(x_1, t\right) \mp \frac{\mu_o^{\pm}}{c_s^{\pm}} \dot{u}_3^{\pm} \mp \frac{\mu_o^{\pm}}{2L_g^{\pm}} u_3^{\pm} + f^{\pm}\left(x_1, t\right), \tag{12}$$

where $\dot{u}_3^{\pm}$ are the velocities in the top and bottom half-spaces evaluated on the weak-plane $x_2 = 0$. In Equation (12) the fourth term $f^{\pm}\left(x_1, t\right)$ is the convolution term that corresponds to the tractions related to the history of the displacements. The convolution over the past slip history in the spectral domain is computed as

$$F^{\pm}\left(k, t\right) = \mp \mu_o^{\pm} \left|k\right| \int_0^t H^{\pm}\left(\left|k\right| c_s^{\pm}\left(t - t'\right)\right) \psi^{\pm}\left(k, t\right) \left|k\right| c_s^{\pm} dt', \tag{13}$$

where $H^{\pm}(Z)$ is the convolution kernel given by

$$H^{\pm}(Z) = \sqrt{1+(\omega^{\pm})^2}\frac{J_1\left(Z\sqrt{1+(\omega^{\pm})^2}\right)}{Z}, \tag{14}$$

with J_1 being the Bessel's function of the first order and first kind. In Equation (14) $\omega^{\pm} = 1/\left(2kL_g^{\pm}\right)$, and is important to note that for the trivial homogeneous bimaterial system with $L_g^{\pm} = \infty$, the convolution kernel derived by Breitenfeld and Geubelle (1998) is obtained. The convolution kernel derived here is a well behaved non-singular function, similar to the other spectral forms derived for various materials (Geubelle and Rice, 1995; Morrissey and Geubelle, 1997; Geubelle et al., 1998; Breitenfeld and Geubelle, 1998; Geubelle and Breitenfeld, 1997; Hwang and Geubelle, 2000; Kulkarni et al., 2007; Pal et al., 2007). The convolution kernel is even with respect to the inhomogeneity length scale $L_g^{\pm}$ and is depicted for three values of the same in Figure 2. The elastodynamic relation (12) is solved numerically, whose details are provided in the next section.

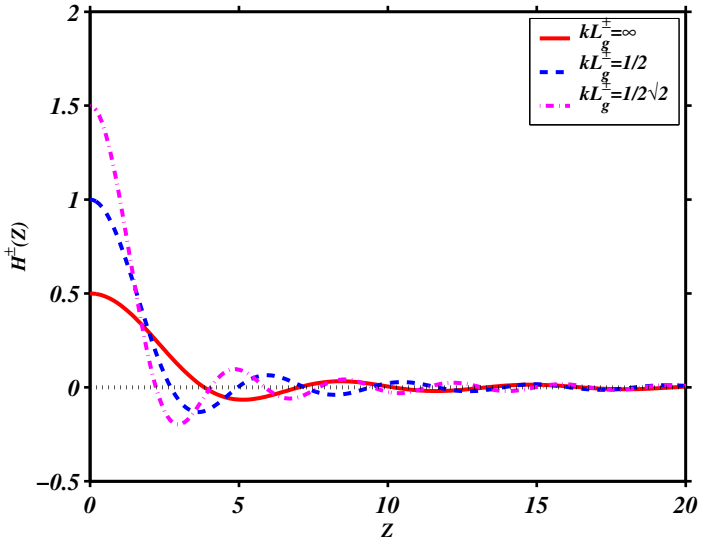

Fig. 2. Convolution kernel for three values of $kL_g^{\pm}$ (with $k = 1$). The convolution kernel has a $\lim_{z\to 0}\left[H^{\pm}(Z)\right] = \left(1+(\omega^{\pm})^2\right)/2$ as shown here.

3 Implementation

In this section we present the implementation specifics of the spectral scheme developed for a functionally graded bimaterial system that was presented in the previous section. The main issues in the numerical implementation of

the spectral scheme are the accurate evaluation of the Fourier modes of the displacements $u_3^{\pm}$, the convolution terms $f^{\pm}$ and the time updating scheme. We use the fast Fourier transform (FFT) algorithm to obtain the numerical Fourier coefficients. The FFT algorithm requires the weak-plane X to be discretized into $N = 2^n$ equally spaced ($\Delta x_1 = X/N$) points on which the Fourier coefficients are obtained numerically as

$$\begin{aligned} u_3^{\pm}(x_1,t) &= \sum_{k=-N/2}^{k=N/2} \psi_{ok}^{\pm} \exp\left(\tfrac{2\pi i k}{X} x_1\right), \\ f^{\pm}(x_1,t) &= \sum_{k=-N/2}^{k=N/2} F_k^{\pm} \exp\left(\tfrac{2\pi i k}{X} x_1\right). \end{aligned} \tag{15}$$

The numerical representation of the Fourier transform introduces an artificial replication as indicated by the above equation, which is represented by the change in the spectral mode number from $k \to 2\pi k/X$. The computation of the convolution integral is similar to the algorithm described in Geubelle and Rice (1995), wherein the pre-integrated, truncated kernel is used to account for the response from the slip history. The second implementation specific is the time update scheme. We use an explicit time stepping scheme, this choice arises from the physics of the problem requiring the time step Δt to be sufficiently small to capture the damage event occurring inside the finite sized cohesive zone ahead of the crack tip. The displacements along the weak-plane are updated as

$$u_3^{\pm}(x_1, t+\Delta t) = u_3^{\pm}(x_1,t) + \Delta t\ \dot{u}_3^{\pm}(x_1,t). \tag{16}$$

From the literature on the implementation of the spectral scheme, it is seen that the time step is chosen as a fraction of the Courant number as

$$\Delta t = \beta \frac{\Delta x_1}{\max\left(c_s^+, c_s^-\right)}, \tag{17}$$

where β is typically chosen to be 0.2 in order to converge temporally and to obtain a numerically stable solution. The above choice of the time step size Δt leads to a condition that the fastest wave takes a minimum of 5 time steps to traverse the distance of Δx_1. The velocities $\dot{u}_3^{\pm}(x_1,t)$ are obtained by solving the elastodynamic equation (12) in conjunction with a cohesive law. The spectral scheme developed here is versatile and can handle any general state-, rate- and/or damage-dependent cohesive model of the form

$$\tau^{\text{strength}} = \tau^*\left(x_1, t, u_3^{\pm}, \dot{u}_3^{\pm}\right). \tag{18}$$

where τ^{strength} is the shear strength inside the cohesive zone. In the present study, the emphasis is to understand the effect of the material property inhomogeneity on the spontaneous crack propagation characteristics and hence we restrict our attention to a simple quasi-linear, damage-dependent cohesive model similar to the one described in Geubelle and Rice (1995). Mathematically the cohesive model can be written as

$$\tau^{\text{strength}} = \tau_c \left(1 - \frac{\left| u_3^+ - u_3^- \right|}{\delta_c} \right) . \tag{19}$$

The above cohesive model is depicted in Figure 3, τ_c corresponds to the

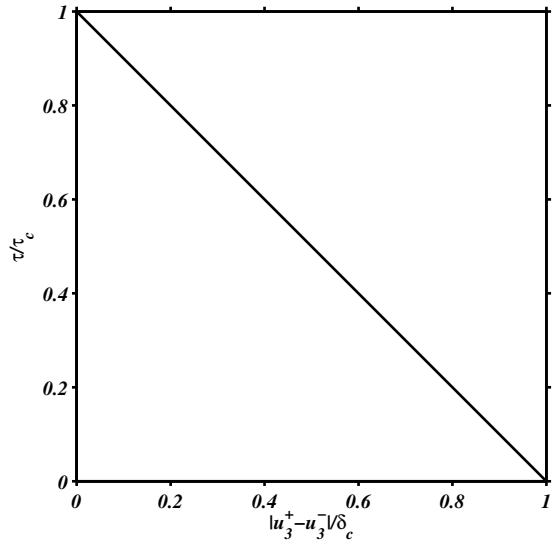

Fig. 3. Damage-dependent cohesive law used in the present study. Here, τ_c and δ_c are the fracture properties of the interface. The fracture toughness at any point on the interface is the area under the traction-separation law.

maximum cohesive strength when the interface is perfectly bonded, that is $\left| u_3^+ - u_3^- \right| = 0$. The critical crack sliding jump δ_c is the maximum permissible crack opening inside the cohesive zone, beyond which a traction-free crack face is created. As mentioned earlier, the above described cohesive zone model is employed in computing the velocities. Owing to the asymmetry of the bimaterial system considered here, we need to compute the velocities of the top and bottom half-spaces independently. The algorithmic procedure is similar to the one described in Geubelle and Breitenfeld (1997). As depicted in Figure 1, the interface/weak-plane comprises of three distinct regions; first is the portion on which the crack is present and the tractions are absent. The second is the region in the immediate vicinity of the crack, that is the cohesive zone. Inside the cohesive zone, both the tractions and displacement jumps are present and are related via a cohesive zone model. The third region is the uncracked region, where the tractions are continuous and no displacement or velocity jump

occurs. The velocities in the uncracked portion of the weak-plane are given by

$$\dot{u}_3^+ = \dot{u}_3^- = \frac{f^+ - f^-}{\frac{1}{\rho^+ c_s^+} + \frac{1}{\rho^- c_s^-}}. \tag{20}$$

The velocities inside the cohesive zone are computed as

$$\dot{u}_3^\pm = \frac{c_s^\pm}{\mu_o^\pm} \left(\tau^o + f^\pm - \tau^{\text{strength}} \right). \tag{21}$$

The computed velocities are used in the explicit time stepping scheme described by Equation (16) to compute the displacements. In comparison with the formulation by Kulkarni et al. (2007) and Pal et al. (2007) the present spectral formulation is more generic as it can handle the inhomogeneities of two half-spaces independently. The present method however is computationally more intensive as two convolution integrals corresponding to the upper and lower half-spaces need to be evaluated separately. As mentioned in Geubelle and Breitenfeld (1997) this additional computation can be overlooked at the advantages the scheme offers. As mentioned in Geubelle and Rice (1995) the convolution integral could be evaluated in a parallel computer, there by decreasing the actual computational time. Similar to the existing spectral schemes the present bimaterial formulation is computationally efficient compared to numerical methods such as finite differences and finite elements. Finite element simulations of the spontaneous interfacial crack growth problem considered in the present study would require a minimum of N^2 degrees of freedom to achieve similar accuracy as obtained by the spectral scheme.

As mentioned earlier, the main aim of the present study is to understand the effects of varying the inhomogeneous material properties independently in the two half-spaces on the spontaneous crack propagation characteristics. We simulated the spontaneous crack propagation using the spectral scheme described thus far. A parametric study was performed by systematically varying the inhomogeneity length scales ($L_g^\pm$) in the two half-spaces. The results from our parametric study are described in the next section.

4 Results and discussion

The primary focus of the present study is to understand the effect of varying the material property inhomogeneity independently in the two half-spaces. We performed a parametric study by systematically varying the inhomogeneity length scales. We used the spectral scheme that is developed in Section 2 to simulate spontaneous crack propagation along the interface of a functionally graded bimaterial system (Figure 1). As described by Lambros et al. (1999)

one of the manufacturing processes to obtain inhomogeneous material property variations is to expose the parent material (such as PMMA, ECO) to ultraviolet (UV) radiation of different time durations. The mechanical properties namely the rigidity modulus and density increases with the duration of the exposure to UV radiation. A desired inhomogeneity length scale (L_g) is obtained by controlling the velocity of the mask during the exposure. In the present study, we assume that the two half-spaces are made of the same parent material, but were exposed to different rates of ultraviolet radiation. This leads to a bimaterial system that will have identical rigidity modulus $\mu_o^{\pm}$ and density $\rho_o^{\pm}$ on the interface (weak-plane). The different exposure rates to UV leads to different inhomogeneity length scales in each of the half-spaces. In the rest of the discussion in this work we assume that the rigidity modulus on the interface to be μ_o=2 GPa, density to be ρ_o=1230 $Kg-m^{-3}$. The above material properties correspond to an untreated sheet of PMMA. The choice of the above mentioned rigidity modulus and density leads to a homogeneous shear wave speed of c_s=1275 $m-s^{-1}$. The weak-plane X (Figure 1) was assumed to be $16a_o$ and was divided into $N = 2048(2^{11})$ equal parts (Δx_1), which was sufficient to achieve spatial convergence. The time step $\Delta t = a_o/(64c_s)$ seconds was used in all our simulations. In order to avoid replication effects from the phantom domains, which is a numerical artifact, we restricted the right crack tip to grow only up to a maximum of $X/2$ ($8a_o$), while the left crack tip was held stationary. The interfacial fracture toughness was set to be G_c = 5 $kJ-m^{-2}$, which was assumed to have been obtained of a critical crack opening displacement $\delta_c = 2\ mm$ and maximum shear strength $\tau_c = 5\ MPa$. A time invariant, uniformly distributed external loading $\tau_o = \tau_c/2$ was applied in all our simulations. Several combinations of the inhomogeneity length scale were used in our parametric study. For the purpose of explaining the results four bimaterial combinations are considered. They are:

A Both the top and bottom half-spaces are made of homogeneous materials with $L_g^{\pm} = \infty$, which is our reference material.
B The bottom half-space is assumed to be a hardening FGM with $L_g^- = 50\delta_c$ and the top is a homogeneous material with $L_g^+ = \infty$.
C The bottom half is a softening FGM with $L_g^- = -50\delta_c$ while the top is again a homogeneous material with $L_g^+ = \infty$.
D Both the half-spaces are made of inhomogeneous materials with the bottom half-space being a hardening FGM ($L_g^- = 100\delta_c$) and the top is a weakening FGM ($L_g^+ = -25\delta_c$).

The above graded bimaterial combinations are schematically shown in Figure 4. We examined the effect of the material property inhomogeneity on the crack sliding displacements by recording snapshots of the displacements while the simulation progressed, which are shown in Figure 5. These snapshots were recorded at regular intervals of $t = 0.4a_o/c_s$ seconds apart. The displacements are normalized with the critical crack opening displacement δ_c. The crack slid-

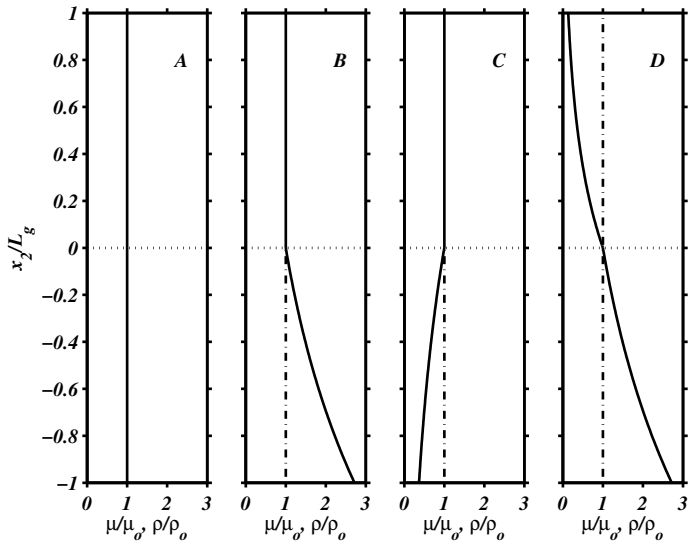

Fig. 4. The functionally graded bimaterial systems described in the results. The homogeneous case (A) is our reference material.

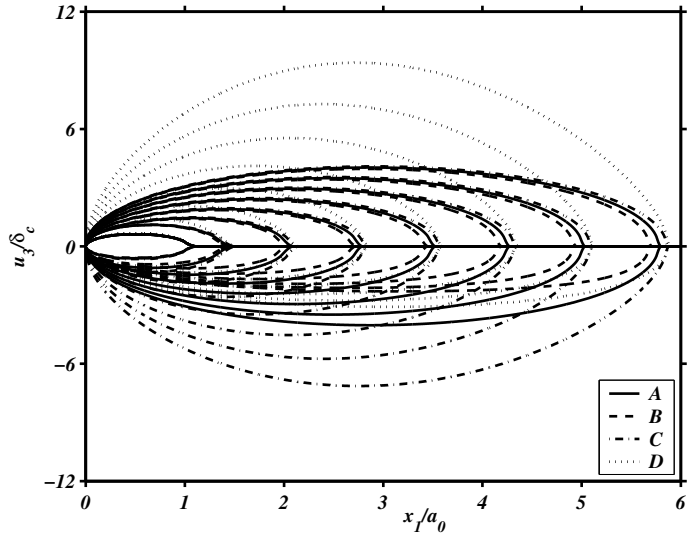

Fig. 5. Snapshots of the crack sliding profiles recorded at regular intervals of $t = 0.4a_o/c_s$ seconds apart. The crack opening is symmetric in the homogeneous case (A), while it is asymmetric in the FGM cases.

ing displacements in the homogeneous material (A) is symmetric about the weak plane as expected. In the bimaterial combination B the crack sliding is affected by the material inhomogeneity in the bottom half. The material becomes more rigid and dense with increase in x_2, which leads to an increase in the fracture resistance and hence the crack opening is lesser in the bottom half as compared with the homogeneous case. While in the upper half-space, the crack sliding displacements are of the same order of magnitude as that of the homogeneous material. Due to the material inhomogeneity in the lower half-space alone the crack tip in the bimaterial case B is seen trailing the

homogeneous material (A) at all time steps. The crack sliding displacements for the third bimaterial combination also exhibits an effect of the material property inhomogeneity. In this bimaterial case the material in the bottom half-space becomes more compliant, which leads to a reduction of the fracture resistance and hence a larger crack opening displacements is observed in the bottom half space as compared to the upper half-space (homogeneous material). The crack tip is ahead in case C as compared to that in the homogeneous (A) and the bimaterial case B. This observation, indicates that the material property inhomogeneity affects the crack propagation velocity, which will be illustrated later. In the bimaterial case D, the material property inhomogeneity is present in both the upper and lower half-spaces. The crack sliding in the lower half is lesser than in the homogeneous material as the material is strengthening, while in the upper half the crack sliding is larger than in the homogeneous material due to the presence of the weakening material. This clearly illustrates that a softening material offers lesser resistance to fracture while the hardening material increase the fracture resistance as seen. The position of the crack tip always leads the homogeneous case as seen, which indicates that the combination of the hardening and softening graded materials considered in case D leads to a decrease of the effective fracture resistance. The above observations are similar to those of Kulkarni et al. (2007) and Pal et al. (2007). The details of the asymmetric opening, lead or lag of

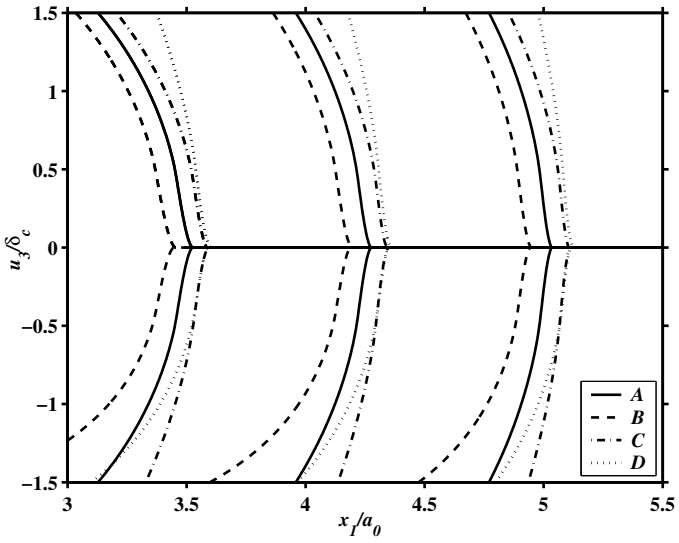

Fig. 6. Magnified view of the crack sliding profiles depicting the details of the cohesive damage for different graded materials. For the sake of clarity the time interval between the successive snapshots is delayed to $0.6a_o/c_s$ seconds.

the crack tip is better visualized by zooming the near-tip details as shown in Figure 6. These snapshots were recorded at $0.6a_o/c_s$ seconds apart for the sake of clarity. From this plot the damage inside the cohesive zone is clearly visible. The extent of the cohesive zone is evaluated by $u_3^+ - u_3^- = \delta_c$ (Dugdale condition). The extents of the cohesive zone are affected by the inhomogene-

ity combinations considered (also illustrated in Figure 10). The crack sliding displacement profiles inside the cohesive zone are affected due to the material property variation. The change in the crack sliding profile inside the cohesive zone also means that the tractions and hence the stresses and power absorbed inside the cohesive zone are affected by the material property inhomogeneity. It is important to note that the fracture parameters namely the critical crack opening displacements δ_c and the maximum shear strength τ_c in the cohesive zone are identical for all the bimaterial combinations considered in our study. We examined the stresses ahead of the cohesive zone tip and found that they were not affected by the material inhomogeneity, which was also observed in the simulations of Pal et al. (2007). From Figure 5 and Figure 6,

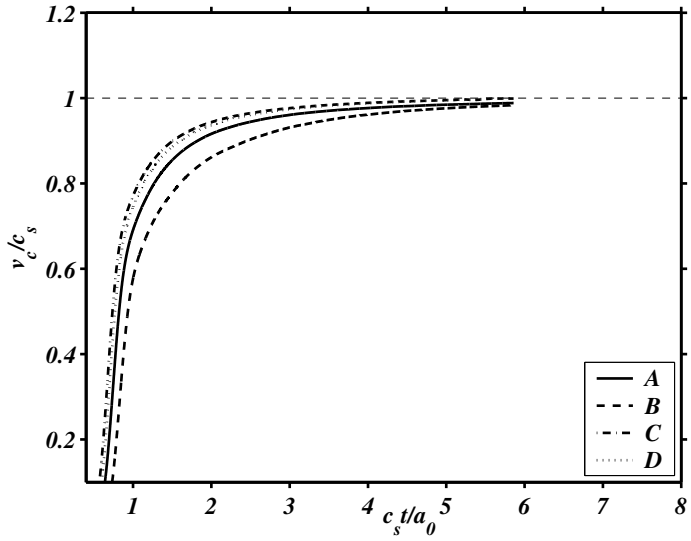

Fig. 7. Evolution of the crack tip velocity for different graded materials. The crack reaches a constant quasi-steady-state velocity equal to the shear wave speed (c_s) for all the material combinations considered.

we see that the crack tip positions are either leading or lagging the reference homogeneous material, indicating that the crack tip velocities are affected by the inhomogeneous material property variations. The crack tip velocity history shown in Figure 7 illustrates this effect. The crack remains stationary until sufficient energy is absorbed in the cohesive zone. The crack accelerates rapidly once it starts to grow and reaches a quasi-steady-state of propagation in all the bimaterial combinations simulated. This is due to the fact that a constantly increasing supply of energy is provided to the system by applying an uniform traction stress on the faces of the expanding crack. The maximum quasi-steady-state velocity of propagation the crack reaches is the shear wave speed (c_s), which is the limiting speed of crack propagation under mode 3 loading conditions. The time instant at which the crack begins propagating is also affected by the material property inhomogeneity. In comparison with the homogeneous case (A), the homogeneous-hardening FGM system (B) delays the start of the crack propagation due to the increase in the fracture

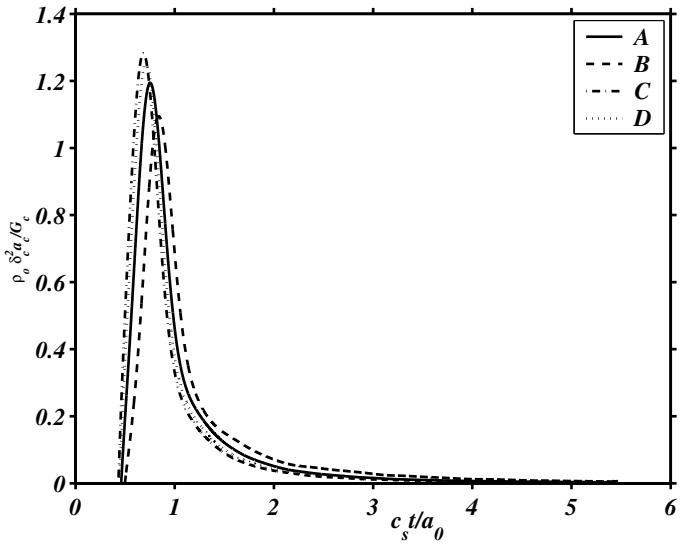

Fig. 8. Crack tip acceleration history for the graded materials. The crack tip acceleration tends to zero after the initial transients diminish reaching a quasi-steady-state of propagation.

resistance. In the bimaterial system of case C the initial growth time is advanced, and in the bimaterial case D the initial growth time is less compared to the homogeneous case (A) and homogeneous-hardening bimaterial system (B). The initial growth time can be controlled by varying the combinations of the inhomogeneity length scale (L_g). The above observations indicate that the material property inhomogeneities also affects the power absorbed inside the cohesive zone, which will be discussed later (Figure 9). The effect of the material inhomogeneity is to alter the crack propagation velocities as seen. The crack propagation velocity is slower in case B while it is faster in case C. The crack tip velocity in bimaterial system C is greater than the homogeneous (A) and homogeneous-hardening bimaterial system (B). As can be seen, only the transient crack propagation velocity seems to be affected, while the quasi-steady-state reached remains unaffected. In order to better visualize the accelerating phase of crack propagation we recorded the crack tip acceleration history depicted in Figure 8. As seen from Figure 7, the crack reaches a quasi-steady-state of propagation for all the combinations of the bimaterial systems studied, which is indicated here by the vanishing accelerations (for $t > 4a_o/c_s$). In the transient phase the crack accelerates faster in the functionally graded bimaterial systems of cases C and D, indicating a reduction in fracture resistance. While in the material combination of case B the crack tip acceleration is slower than in the homogeneous material. The crack reaches its peak acceleration first in case C, followed by the bimaterial case D, homogeneous material (A) and the last in the hardening-homogeneous system of case B. The magnitude of the crack tip accelerations follows a similar trend, in which the maximum is achieved in the case C and the least being in case B. From the crack tip velocity and acceleration histories, we see that the

propagation velocity increases for bimaterial systems that include a softening functional graded material in one of the half-spaces. Similar observations of increase in the propagation velocity were made by Jain and Shukla (2006), in their experiments.

As indicated by the crack sliding displacements (Figure 5 and 6), histories of the crack tip velocities and accelerations, the power absorbed inside the cohesive zone seems to be affected by the material property inhomogeneity. This can be better visualized by tracking the history of the power absorbed (Figure 9). The power absorbed during the cohesive damage process is defined

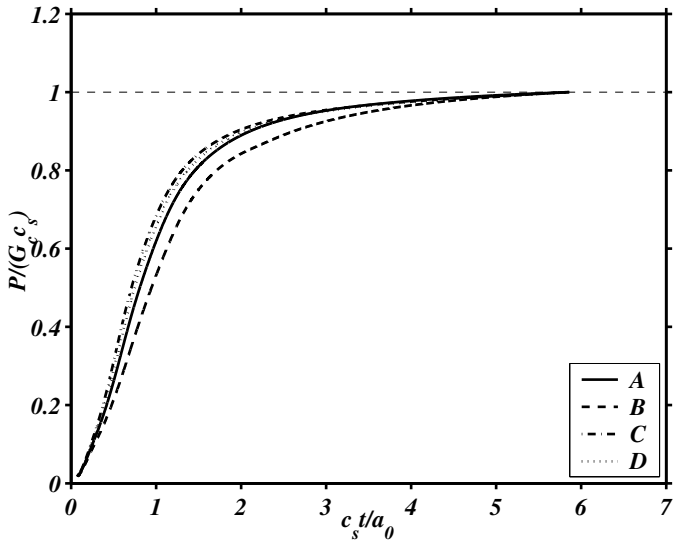

Fig. 9. History of the rate of energy (power) absorbed in the cohesive zone for different graded materials. The absorbed energy reaches a constant of $G_c c_s$ in the quasi-steady-state of propagation regime, irrespective of the type and extent of the material inhomogeneity.

as

$$P(t) = \int_0^{L_c(t)} \tau(x_1, t) |\dot{u}_3^+(x_1, t) - \dot{u}_3^-(x_1, t)| dx_1, \tag{22}$$

where $L_c(t)$ is the length of the cohesive zone and $\tau(x_1, t)$ are the cohesive tractions. As the crack reaches a quasi-steady-state of propagation (Figure 7 and 8), a constant power of $G_c c_s$ is absorbed in the cohesive zone and hence used in normalizing the power. The power absorbed in the cohesive zone is lesser in the hardening-homogeneous bimaterial combination (B). This can be attributed to the fact that the material combination of case B offers a higher fracture resistance, leading to a reduction in the velocity of crack propagation (Figure 7) and hence the power absorbed. In other words, the opening displacements are smaller in case B (Figure 5 and 6) compared to the other

three cases, leading to lesser velocity jumps ($\dot{u}_3^+ - \dot{u}_3^-$) in the cohesive zone and thereby reducing the power absorbed. In the graded bimaterial considered in case C and D, the fracture resistance is effectively reduced due to the material inhomogeneity on either side of the weak-plane, leading to a smaller sized cohesive zone, larger crack opening and velocity jumps and hence leading to an increase in the power absorbed. Similar observations were made in the study of unsymmetric (Kulkarni et al., 2007) and symmetric (Pal et al., 2007) graded materials. The observations of Lambros et al. (1999) in their mode 1 crack growth experiments also support our theoretical predictions. The magnified crack sliding displacements (Figure 6) indicated that the size

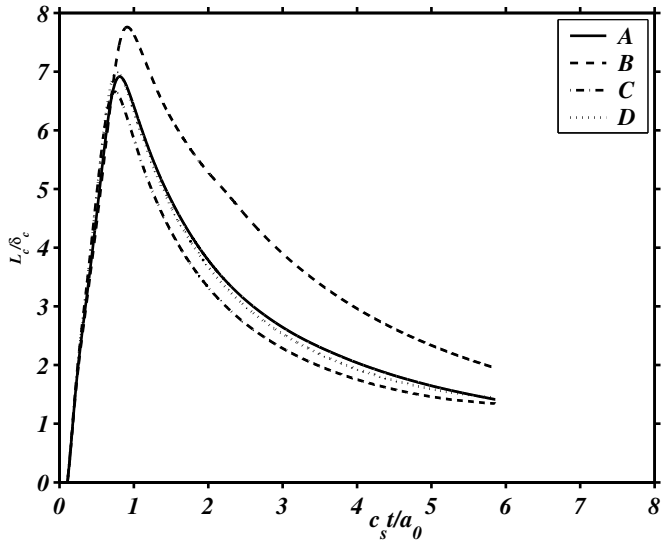

Fig. 10. History of the length of the cohesive zone for different bimaterial systems. The cohesive zone size increases until sufficient energy is absorbed in the cohesive zone. Once the crack tip starts accelerating the length of the cohesive zone reduces and finally reaches a constant.

of cohesive zone is affected by the material property inhomogeneity. Figure 10 depicts the time history of the length of the cohesive zone, for different inhomogeneous bimaterial combinations. The cohesive zone size initially increases rapidly in the transient phase for all the material combinations studied here. This is due to the fact that the crack tip remains stationary until sufficient energy (G_c) is absorbed before beginning to propagate. Once the crack tip begins to accelerate the length of the cohesive zone reduces in size until it reaches almost a constant. When the cohesive zone length remains invariant with time, a constant power is absorbed in the cohesive zone indicating the attainment of a quasi-steady-state of propagation. Due to the increased fracture resistance of the combination in case B the cohesive zone is longer compared to the other three bimaterial combinations. The history of the cohesive zone length of case D is almost same as that of the homogeneous material as seen. In our parametric study, we have observed that for a few combinations of the material inhomogeneities in the two half-spaces, crack propagation behavior

similar to that of a homogeneous material is observed. However, the mechanics of cohesive damage, power absorbed are distinctly different indicating the effect of the inhomogeneity. As observed earlier, the combination of a softening material with a homogeneous material (C) was the least resistant to fracture among the four cases, which is also indicated by the cohesive zone length for this case. Finally we summarize our results by plotting the contours

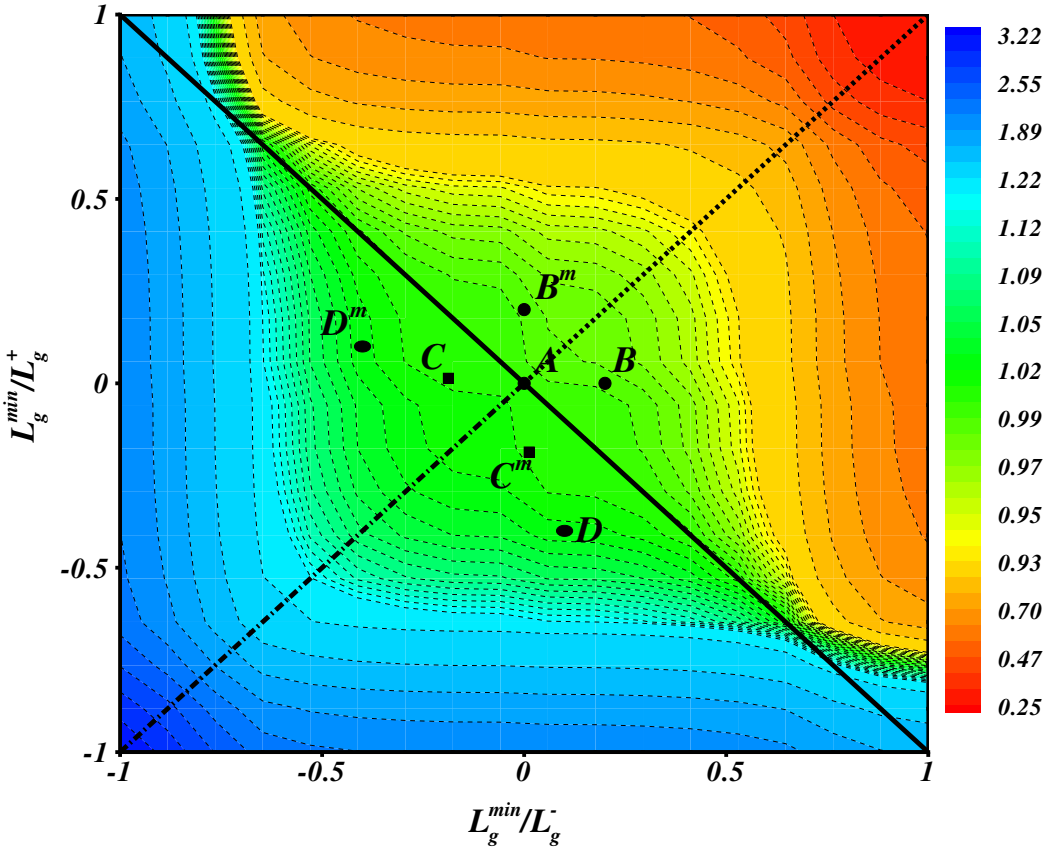

Fig. 11. Contours of maximum crack opening displacement for several bimaterial combinations. The opening displacements were extracted after the crack propagation reached a quasi-steady-state of propagation ($t > 3a_o/c_s$ seconds). The crack opening displacements are normalized with those from the reference homogeneous material A. The bimaterial combinations B to D (Figure 4) and their mirror images (superscript 'm') are marked here.

of the maximum crack sliding jumps obtained from all the bimaterial combinations we have simulated. In all of the bimaterial systems considered in our study, the crack propagation reached a quasi-steady-state of propagation after about $3a_o/c_s$ seconds. This corresponds to the time the crack takes to grow three times its original length, if propagating at a constant speed of c_s $m - s^{-1}$. In other words, quasi-steady-state of propagation is attained after

the crack has grown to approximately thrice its initial size. The crack opening displacements are defined as $\delta = u_3^+ - u_3^-$ and the maximum crack opening displacements are extracted from the data of the crack profile snapshots (Figure 5). For the sake of comparison, the maximum opening displacements are normalized by the maximum crack opening displacements from the reference homogeneous material (A). These contours were obtained by varying the inhomogeneity length scales in the two half-spaces as $L_g^{\pm} = \left(L_g^{min}, \infty\right)$. The most severe inhomogeneity was chosen to be $L_g^{min} = 10\ \delta_c$, which ensured that the material properties did not vary inside the cohesive zone ($\delta \leq \delta_c$). A total of 243 (9 $L_g^+ \times 9\ L_g^- \times 3$ quadrants) bimaterial combinations were simulated to obtain this plot. The x-axis corresponds to the inhomogeneity in the lower half-space (L_g^-) and the y-axis corresponds to inhomogeneous material property variation in the upper half-space (L_g^+). The axes are shown as reciprocal of $L_g^{\pm}$ in order to accommodate the large range of inhomogeneity length scales. It is important to note that all the bimaterial combinations considered here have identical interfacial fracture toughness (G_c) and material properties (μ_o and ρ_o). The four bimaterial combinations (Figure 4) described so far in the results are marked on the contours. The mirror images of the bimaterial combinations (B to D) are indicated by a superscript m. As mentioned earlier the unsymmetric material property variation considered in Kulkarni et al. (2006) is a special case of the general bimaterial analysis presented here. The unsymmetric functionally graded material combinations are indicated by the main diagonal (solid) line. The skew diagonal line corresponds to the symmetric softening (dash-dot) and hardening (dashed) functionally graded materials considered in Pal et al. (2006). Contours of the maximum opening displacements are symmetric about the symmetric functionally graded material (skew diagonal) line, which is expected as the bimaterial combinations are mirror reflections on either side of the symmetric (skew diagonal) line. Maximum opening displacements occur in symmetric softening material (bottom left corner, [-1,-1]) and the least opening is seen in the symmetric hardening material (top right corner, [1, 1]). The opening displacements in the unsymmetric graded materials is larger compared to the homogeneous indicating that the deformations closely resemble a symmetric softening material. Similar observations were made in the study of Pal et al. (2006). The effect of including a hardening type graded material in either of the half-spaces in the bimaterial system is to reduce the fracture resistance indicated by the reduction in the opening displacements. When a softening material is included in the bimaterial system, crack opening displacements increase signifying a decrease in the fracture resistance. The crack opening displacements are least affected for larger values of the inhomogeneity length scale $L_g^{\pm}$, which is indicated by an elliptical region surrounding the origin where the displacements are almost equal to that in the homogeneous material. The bimaterial combinations B to D described thus far, lie in the above mentioned less affected region. The crack propagation characteristics, such as velocities (Figure 7), accelerations

(Figure 8) and power absorbed (Figure 9) are affected by the inhomogeneous material property variations as seen previously. The major axis of the less affected elliptical region is oriented along the unsymmetric FGM (diagonal) line indicating that the effect of inhomogeneity is less pronounced for unsymmetric bimaterial combinations (say, hardening in the upper half and softening in the lower half or vice-versa). On the other hand, the crack opening displacements are more sensitive to the material property inhomogeneity when symmetric combinations make up the bimaterial system. As mentioned earlier, crack propagation characteristics are most severely affected in the symmetric bimaterial combinations with identical inhomogeneity length scales in the two half-spaces (skew diagonal line).

5 Conclusions

We have developed a special form of the spectral scheme to simulate 2D planar crack propagation along the interface of inhomogeneous bimaterial systems. The scheme developed is versatile, similar to its predecessors, in which a variety of traction-separation (cohesive zone) laws or friction laws can be used. The developed spectral scheme was used to perform a parametric study by assuming that the inhomogeneity length scale (L_g) varies independently in either of the two half-spaces. We draw the following conclusions from our parametric study:

(1) Bimaterial combinations comprising at least one softening graded half-space will always decrease the fracture resistance, indicated by the larger crack opening and faster crack propagation velocities. The fracture resistance of the bimaterial system increases when one of the half-spaces is a hardening functionally graded material, which is indicated by the reduced crack opening displacement and slower crack propagation velocities.

(2) The effects of the material property inhomogeneity on the crack propagation characteristics are more pronounced in bimaterial systems comprising of symmetric combinations. These are obtained by combining softening-softening or hardening-hardening half-spaces. The inhomogeneity effect is most severe for symmetric FGMs with identical property gradients ($L_g^+ = L_g^-$).

(3) The cohesive zone size (ductility) increases with increase in the effective fracture resistance, while the power absorbed decreases due to the reduced crack opening velocity jumps. This occurs in bimaterial combinations containing atleast one hardening FGM half-space. On the other hand, ductility decreases and the power absorbed increases when a softening graded material is included in the system.

(4) The material inhomogeneity affects both the crack opening displacements and cohesive tractions inside the cohesive zone. However, the stresses

ahead of the cohesive zone tip are not affected by the inhomogeneous material property variations.

Acknowledgments

Part of this work has been supported by the FAST young scientist award funded by the Department of Science and Technology (DST), India. Kubair acknowledges the support from the All India Council for Technical Education (AICTE), through their young teacher award. Some of the simulations presented in this article have been performed on the computers available at the Supercomputer Education and Research Center (SERC), located on the Indian Institute of Science, Bangalore campus.

References

Abanto-Bueno, J., Lambros, J., 2006. An experimental study of mixed mode crack initiation and growth in functionally graded materials. Experimental Mechanics 46 (2), 179–196.

Breitenfeld, M., Geubelle, P., 1998. Numerical analysis of dynamic debonding under 2d in-plane and 3d loading. International Journal of Fracture 93 (1-4).

Camacho, G., Ortiz, M., 1996. Computational modelling of impact damage in brittle materials. International Journal of Solids and Structures 33 (20-22).

Chen, C., Takita, K., Ishiguro, S., Honda, S., Awaji, H., 2005. Fabrication on porous alumina tube by centrifugal molding. Journal of the European ceramic Society 25 (14), 3257–3264.

Delale, F., Erdogan, F., 1983. The crack problem for a non-homogeneous plane. Journal of Applied Mechanics-Transactions of the ASME 50 (3), 609–614.

Eischen, J., 1987. Fracture of nonhomogeneous materials. International Journal of Fracture 34 (1).

Feng, W., Su, R., Jiang, Z., 2005. Torsion impact response of a cylindrical interface crack between a functionally graded interlayer and a homogeneous cylinder. Composite Structures 68 (2), 203–209.

Gasik, M., Zhang, B., der Biest, O. V., Vleugels, J., Put, S., 2003. Design and fabrication of symmetric fgm plates. Functionally Graded Materials VII Materials Science Forum 423-4, 23–28.

Geubelle, P., Baylor, J., 1998. Impact induced delamination of composites:a 2-d simulation. Composites Part B- Engineering 29 (5).

Geubelle, P., Breitenfeld, M., 1997. Numerical analysis of dynamic debonding under anti-plane shear loading. International Journal of Fracture 85 (3), 265–282.

Geubelle, P., Danyluk, M., Hilton, H., 1998. Dynamic mode 3 fracture in

viscoelastic media. International Journal of Solids and Structures 35 (9-10), 761–782.

Geubelle, P., Rice, J., 1995. A spectral method for three-dimensional elastodynamic fracture problems. Journal of the Mechanics and Physics of Solids 43 (11), 1791–1824.

Hashmi, S., 2006. Attaining a controlled graded distribution of particles in polymerizing fluid for functionally graded materials. Journal of Applied polymer science 99 (6), 3009–3017.

Hosson, J. D., Ocelik, V., 2003. Functionally graded materials produced with higher power lasers. Thermec'2003, Pts 1-5 Materials Science Forum 426-4, 123–130.

Hwang, C., Geubelle, P., 2000. A spectral scheme to simulate dynamic fracture problems in composites. CMES- Computer Modelling in Engineering & Sciences 1 (4), 44–45.

Jain, N., Shukla, A., 2006. Mixed mode dynamic fracture in particulate reinforced functionally graded materials. Experimental Mechanics 46 (2), 137–154.

Jiang, W., Wang, L., Chen, L., Qin, C., 2005. A novel fabrication method of multiphase nanoceramics -in-situ reactive sintering via sps(isr-sps). Rare Metal Materials and Engineering 34 (1), 367–370.

Kandula, S., Abanto-Bueno, J., Geubelle, P., Lambros, J., 2005. Cohesive modeling of dynamic fracture in functionally graded materials. International Journal of fracture 132 (3), 275–296.

Kato, K., Kurimoto, M., Shumiya, H., Adachi, H., Sakuma, S., Okubo, H., 2006. Application of functionally graded material for solid insulator in gaseous insulation system. IEEE Transactions on dielectrics and electrical insulation 13 (2), 362–372.

Kirugulige, M., Tippur, H., 2006. Mixed mode dynamic crack growth in functionally graded glass-filled epoxy. Experimental Mechanics 46 (2), 269–281.

Kitey, R., Tippur, H., 2005. Dynamic crack growth in particulate bimaterials having discrete and diffuse interfaces: Role of microstructure. Engineering Fracture Mechanics 72 (18), 2721–2743.

Koizumi, M., 1997. Fgm activities in japan. Composites part B-Engineering 28 (1-2), 1–4.

Koizumi, M., Niino, M., 1995. Overview of fgm research in japan. MRS Bulletin 20 (1), 19–21.

Kondo, H., Yokoyama, A., Omori, M., Ohkubo, A., Hirai, T., Watari, F., Uo, M., Kawasaki, T., 2004. Fabrication of titanium nitride/apatite functionally graded implants by spark plasma sintering. Materials Transactions 45 (11), 3156–3162.

Kubair, D., Geubelle, P., 2003. Comparative analysis of extrinsic and intrinsic cohesive models of dynamic fracture. International Journal of Solids and Structures 40 (15), 3853–3868.

Kubair, D., Geubelle, P., Huang, Y., 2003. Analysis of a rate-dependent cohesive model for dynamic crack propagation. Engineering Fracture Mechanics

70 (5), 685–704.

Kulkarni, M., Pal, S., Kubair, D., 2007. Mode-3 spontaneous crack propagation in unsymmetric functionally graded materials. International Journal of Solids and Structures 44 (1), 229–241.

Lambros, J., Rosakis, A., 1995. Shear dominated transonic interfacial crack-growth in a bimaterial. 1. experimental-observations. Journal of the Mechanics and Physics of Solids 43 (2), 169–188.

Lambros, J., Santare, M., Sapna, G., Li, H., 1999. A novel technique for the fabrication of laboratory scale model functionally graded materials. Experimental Mechanics 39 (3), 184–190.

Lee, H., Choi, H., 2006. Effects of graded properties on the impact response of an interface crack in a coating-substrate system subjected to antiplane deformation. Zamm Zeitschrift fur Angewandte Mathematik und Mechanik 86 (2), 110–119.

Ma, L., Wu, L., Guo, L., 2005. On the moving griffith crack in a nonhomogeneous orthotropic strip. International Journal of Fracture 136 (1-4), 187–205.

Marur, P., Tippur, H., 2000. Dynamic response of bimaterial and graded interface cracks under impact loading. International Journal of Fracture 103 (1), 95–109.

Melgarejo, Z., Suarez, O., Sridharan, K., 2006. Wear resistance of a functionally-graded aluminum matrix composite. Scripta Materialia 55 (1), 95–98.

Mikumo, T., Hirahara, K., Miyatake, T., 1987. Dynamic fault rupture processes in heterogeneous media. Tectonophysics 144 (1-3), 19–36.

Morrissey, J., Geubelle, P., 1997. A numerical scheme for mode iii dynamic fracture problems. International Journal for Numerical Methods in Engineering 40, 1181–1196.

Movchan, B., Yakovchuk, K., 2004. Graded thermal barrier coatings, deposited by *EB-PVD*. Surface and Coatings Technology 188, 85–92.

Muller, E., Drasar, C., Schilz, J., Kaysser, W., 2003. Functionally graded material for sensor and energy applications. Material Science and Engineering A-Structural Material Properties Microstructures and Processing 362 (1-2), 17–39.

Pal, S., Kulkarni, M., Kubair, D., 2007. Mode-3 spontaneous crack propagation in symmetric functionally graded materials. International Journal of Solids and Structures 44 (1), 242–254.

Parameswaran, V., Shukla, A., 2002. Asymptotic stress fields for stationary cracks along the gradient in functionally graded materials. Transactions of the ASME, Journal of Applied Mechanics 69 (3), 240–243.

Pine, M., Bruck, H., 2006. Pressureless sintering of particle-reinforced metal-ceramic composites for functionally graded materials: part 1 porosity reduction models. Acta Materialia 54 (6), 1457–1465.

Pompe, W., Worch, H., Epple, M., Friess, W., Gelinsky, M., Greil, P., Hempel, U., Scharnweber, D., Schulte, K., 2003. Functionally graded materials for

biomedical applications. Material Science and Engineering A-Structural Material Properties Microstructures and Processing 362 (1-2), 40–60.

Put, S., Vleugels, J., Anne, G., Biest, O., 2003. Functionally graded hardmetals with a continuously graded symmetrical profile. Material Science Forum 423-425, 33–38.

Schulz, U., Peters, M., Bach, F., Tegeder, G., 2003. Graded coatings for thermal, wear and corrosion barriers. Materials Science and Engineering A-Structural Materials Properties Microstructure and processing 362 (1-2), 61–80.

Suresh, S., Mortensen, A., 1998. Fundamentals of Functionally Graded Materials. Institute of Materials, London.

Tilbrook, M., Moon, R., Hoffman, M., 2005. Finite element simulations of crack propagation in functionally graded materials under flexural loading. Engineering fracture Mechanics 72 (16), 2444–2467.

van Zyl, W., Carton, E., Raming, T., ten Elshof, J., Verweij, H., 2005. Dynamic shock compaction of a zro2-ruo2 electronic nanocomposite: toward functionally graded materials. Physica Status Solidi A-Applications and Materials Science 202 (12), R132–R134.

Watanabe, Y., Kim, I., Fukui, Y., 2005. Microstructures of functionally graded materials fabricated by centrifugal solid-particle and in-situ methods. Metals and Materials International 11 (5), 391–399.

Watari, F., Yokoyama, A., Omori, M., Hirai, T., Kondo, H., Uo, M., Kawasaki, T., 2004. Biocompatability of materials and development to functionally graded implant for bio-medical application. Composites Science and Technology 64 (6), 893–908.

Witvrouw, A., Mehta, A., 2005. The use of functionally graded poly-sige layer for mems applications. Functionally Graded Materials VIII Materials Science Forum 492-493, 225–260.

Wosko, M., Paszkiewicz, B., Piasecki, T., Azyszka, A., Paszkiewicz, R., Tlaczala, M., 2005. Application of functionally graded materials in optoelectronic devices. Optica Applicata 35 (3), 663–667.

Xu, L., Huang, Y., Rosakis, A., 2003. Dynamic crack deflection and penetration at interfaces in homogeneous materials: experimental studies and model predictions. Journal of the Mechanics and Physics of Solids 51 (3), 461–486.

Xu, X., Needleman, A., 1994. Numerical simulations of fast crack growth in brittle solids. Journal of the Mechanics and Physics of Solids 42 (9), 1397–1434.

Yang, B., RaviChandar, K., 1996. On the role of the process zone in dynamic fracture. Journal of the Mechanics and Physics of Solids 44 (12), 1955–1976.

Zhang, B., Gasik, M., Facchini, A., Pressacco, M., Dallapria, P., Posocco, S., 2005. Computer-integrated safe design of fgm component for hip replacement prosthesis. Functionally Graded Materials VIII Materials Science Forum, 492–493:483–487.